PROCEEDINGS OF SCIENCE

Search for the $K_L^0 \to \pi^0 \nu\bar{\nu}$ at E391a Experiment

Hideki Morii[*†]
Department of physics, Kyoto University, Kyoto, 606-8502 Japan
E-mail: moriih@scphys.kyoto-u.ac.jp

KEK E391a is the first experiment dedicated to the $K_L^0 \to \pi^0 \nu\bar{\nu}$ decay. Since the theoretical uncertainty in the branching ratio of this mode is small, it provides a good testing ground of the SM and beyond. We performed three physics runs as Run-1, Run-2 and Run-3. An upper limit on the branching ratio for the decay is set to be 6.8×10^{-8} at the 90% confidence level from Run-3 data.

2009 KAON International Conference KAON09,
June 09 - 12 2009
Tsukuba, Japan

[*]Speaker.

[†]E391a Collaboration : J. K. Ahn, Y. Akune, V. Baranov, K. F. Chen, J. Comfort, M. Doroshenko, Y. Fujioka, Y. B. Hsiung, T. Inagaki, S. Ishibashi, N. Ishihara, H. Ishii, E. Iwai, T. Iwata, I. Kato, S. Kobayashi, S. Komatsu, T. K. Komatsubara, A. S. Kurilin, E. Kuzmin, A. Lednev, H. S. Lee, S. Y. Lee, G. Y. Lim, J. Ma, T. Matsumura, A. Moisseenko, H. Morii, T. Morimoto, Y. Nakajima, T. Nakano, H. Nanjo, N. Nishi, J. Nix, T. Nomura, M. Nomachi, R. Ogata, H. Okuno, K. Omata, G. N. Perdue, S. Perov, S. Podolsky, S. Porokhovoy, K. Sakashita, T. Sasaki, N. Sasao, H. Sato, T. Sato, M. Sekimoto, T. Shimogawa, T. Shinkawa, Y. Sugaya, A. Sugiyama, T. Sumida, S. Suzuki, Y. Tajima, S. Takita, Z. Tsamalaidze, T. Tsukamoto, Y. C. Tung, Y. Wah, H. Watanabe, M. L. Wu, M. Yamaga, T. Yamanaka, H. Y. Yoshida, and Y. Yoshimura

© Copyright owned by the author(s) under the terms of the Creative Commons Attribution-NonCommercial-ShareAlike Licence.

PoS(KAON09)046

1. Introduction

The decay $K_L^0 \to \pi^0\nu\bar{\nu}$ occurs via loop diagrams that change the quark flavor from strange to down. It violates CP symmetry directly, and the amplitude is proportional to the imaginary part of the Cabbibo-Kobayashi-Maskawa matrix elements in the standard model (SM). Since the theoretical uncertainty in the branching ratio is small and controlled, it provides a good testing ground of the SM and beyond [1]. The branching ratio $Br(\ K_L^0 \to \pi^0\nu\bar{\nu}\ )$ is predicted to be $(2.49 \times 0.39) \pm 10^{-11}$ [2]. The best limit by the previous experiment was 5.9×10^{-7} [3].

KEK E391a is the first experiment dedicated to the $K_L^0 \to \pi^0\nu\bar{\nu}$ decay. The data taking of E391a is divided into three periods as Run-1, Run-2 and Run-3. The current experimental limit for the branching fraction of this decay mode is 6.7×10^{-8} at 90% confidence level, which is obtained by full sample of Run-2 data [4]. The main issue of this letter is analyzing Run-3 data sample based on better understanding to background sources.

2. Experimental method

In the present experiment, neutral kaons were produced by 12 GeV protons incident on a 0.8-cm-diameter and 6-cm-long platinum target. The proton intensity was typically 2×10^{12} per spill coming every 4 sec. The neutral beam [5], with a solid angle of 12.6 μstr, was defined by a series of six sets of collimators and a pair of sweeping magnets aligned at a production angle of 4 degrees. A 7-cm-thick lead block and a 30-cm-thick beryllium block were placed between the first and second collimators to reduce beam photons and neutrons. The K_L^0 momentum peaked around 2 GeV/c at the entrance of the detector, 11 m downstream from the target.

Figure 1 shows the cross-sectional view of the E391a detector. K_L^0's entered from the left side, and the detector components were cylindrically assembled along the beam axis. Most of them were installed inside the vacuum tank to minimize interactions of the particles before detection. The electromagnetic calorimeter, labeled "CsI", measured the energy and position of the two photons from π^0. It consisted of 496 blocks of $7\times7\times30$ cm^3 undoped CsI crystal and 80 specially shaped CsI blocks used in the peripheral region, covering a 190 cm-ϕ circular area. To allow beam particles to pass through, the calorimeter had a 12×12 cm^2 hole at the center. The main barrel (MB) and front barrel (FB) counters consisted of alternating layers of lead and scintillator sheets with total thicknesses of 13.5 X_0 and 17.5 X_0, respectively, and surrounded the decay region. To identify charged particles entering the calorimeter, scintillation counters (CV) hermetically covered the front of the calorimeter. It consisted of a plastic scintillator hodoscope that were placed 50 cm upstream of the calorimeter and four 6-mm-thick scintillator plates that were located parallel to the beam axis between the hodoscope and the calorimeter. Multiple collar-shaped photon counters (CC00, CC02-07) were placed along the beam axis to detect particles escaping in the beam direction. CC02 was a shashlik type lead-scintillator sandwich counter, and was located at the upstream end of the K_L^0 decay region. CC03 filled the volume between the beam hole and the innermost layers of the CsI blocks in the calorimeter. The vacuum region was separated by a thin multi-layer film ("membrane") into the beam and detector regions. This kept the decay region at 1×10^{-5} Pa despite some outgassing from the detector.

PoS(KAON09)046

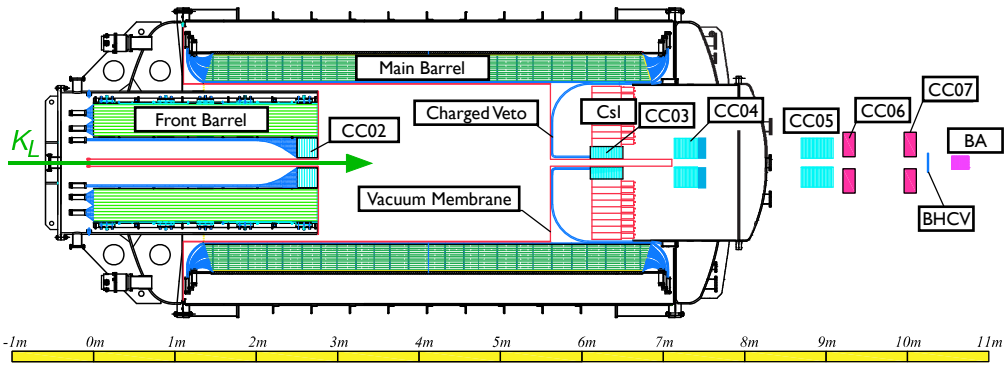

Figure 1: Schematic cross-sectional view of the E391a detector. "0m" in the scale corresponds to the entrance of the detector.

3. Halo neutron background

In Run2 analysis, we found that halo neutron induced background takes the dominant role in our experiment. Halo neutron background is the events due to the neutrons in the halo of the neutral beam ("halo neutrons").

The background was categorized into three types. The first type was due to π^0's produced in the interaction of halo neutrons with the upstream CC02 collar counter ("CC02 BG"). Ideally, their Z position should be reconstructed properly at CC02, *i.e.*, outside the signal box. However, they can enter the signal region when the energy of either photon was mismeasured due to shower leakage or photo-nuclear interactions in the calorimeter.

The second type of neutron-induced background was due to neutron interactions with the CV ("CV BG"). This background should also be reconstructed properly at the Z position of the CV, *i.e.*, outside the signal box. However, events can shift upstream when either cluster was overlapped by other associated particles and thereby mismeasured, or when one of the clusters (or both) was in fact not due to a photon from π^0.

The third type of neutron-induced background was due to η's produced by the halo through interactions with the CV ("CV-η BG"). Since the Z vertex position was calculated by assuming the π^0mass, η's were reconstructed about four times farther away from the calorimeter, and they can fall into the signal box.

To evaluate these three types of neutron-induced background, two steps of Monte-Carlo simulation is carried out. The first step is done by fluka simulation, which is to reproduce hadronic interaction between halo neutron and detectors. The second step is done by geant3 simulation, which is to reproduce electro-magnetic shower in CsI calorimter.

The reproductivity of fluka simulation is determined by data obtained in a dedicated run for this study ("Al plate run"), in which a 0.5-cm-thick aluminum plate was inserted to the beam at 6.5 cm downstream of the rear end of CC02. Figure 2 demonstrates the simulation, which reproduced the invariant mass distribution (from π^0mass to η mass) of the events with two photons in the calorimeter from the Al plate run.

PoS(KAON09)046

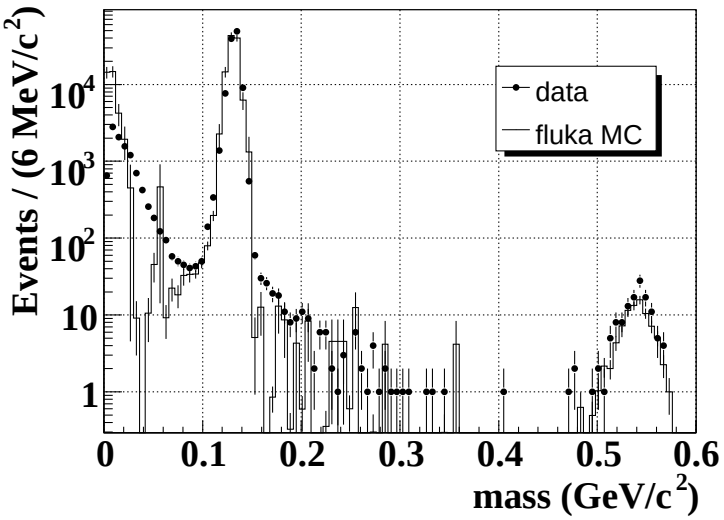

Figure 2: Reconstructed invariant mass distribution of the two photon events in the Al plate run. Points show data and solid line shows fluka simulation. Peak in 0.14 GeV/c^2 shows π^0, and in 0.55 GeV/c^2 shows η respectively.

4. Optimization for event selection

Basis of our event selection is described in refs [4, 6]. Event selection consists of two types; one is particle veto with veto detectors, and the other is kinematic selections. For veto cuts, order of 1 MeV threshold is applied for whole detector system. For kinematic cuts, further optimization from our previous analysis is done to obtain better sensitivity.

Principle of this optimization was keeping S/N as same level as our previous result in Run2 analysis, and maximizing the acceptance. During optimization, signal box was masked both for Run2 and Run3 data in order to avoid biasing. The cut optimization is done in three way; introducing new cut for CV-η BG, replacing several cuts and automatic parameter tuning.

The new cut is implemented for CV-η BG, using the cluster shape information obtained in the CsI calorimeter. Since η particle is produced in CV which is near the CsI, γ produced from η decay tends to have shallow incident angle to the CsI face. This results in wider γ cluster compared to its energy. So, new cut is implemented for this separation using neural network algorithm. Figure 3 shows the performance of this cut against CV-η BG. In the right figure, CV-η BG (shown in black dots) is rejected effectively, with keeping acceptance to signal (shown in color).

After implementing new cuts and parameter optimization, we obtained 46% increase in signal acceptance, keeping S/N as same level as Run2 analysis, as summarized in Table 1.

5. Background estimation

After optimization, number of background is estimated for each categories. For CC02 BG, we estimate 0.15 ± 0.05 event. In this type, the effect of photo-nuclear and shower leakage has

PoS(KAON09)046

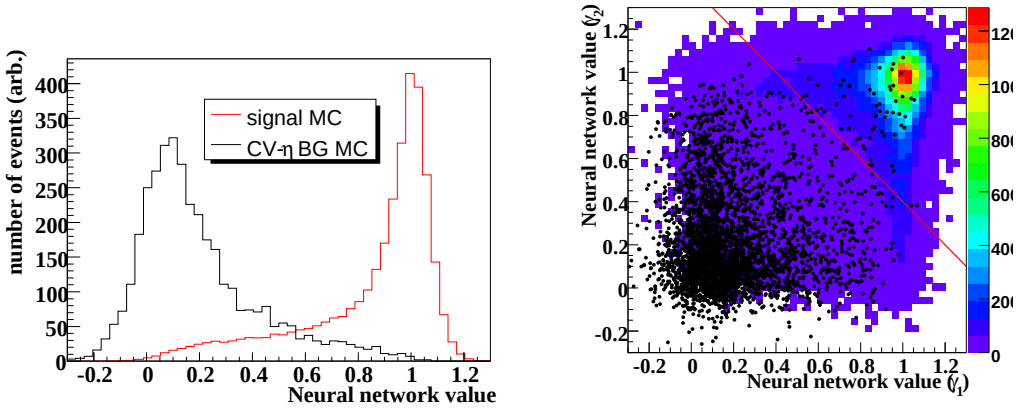

Figure 3: Rejection power of the cluster shape neural network cut. Left figure shows the discriminant value obtained by neural network for signal mode (in red) and CV-η background (in black), respectively. Right figure shows the correlation of discriminant for two photons. Signal mode is shown in colored contour, and CV-η is shown in black dots. Events under red line are rejected.

condition	Signal acceptance	S/N (arbitrary unit)
Run-2 previous cut set	0.67%	5054
New cut set	0.98% (+46%)	5105

Table 1: Acceptance and S/N with previous and new cut set. Acceptance to the signal mode increased by 46% with keeping S/N same level compared to our Run-2 previous result.

the similar level contribution to background. For CV π^0BG, we had no event remaining inside the signal box after applying all cuts with roughly 7 times statistics to the Run-3 data. Thus, we set upper limit for this process as < 0.15. The number of CV-η BG is estimated as 0.14 ± 0.07.

The main background source from K_L^0 decays is the $K_L^0 \to \pi^0\pi^0$ mode, whose branching ratio is 8.7×10^{-4}. There are four photons in the final state, and if two of them escape detection, $K_L^0 \to \pi^0\pi^0$ can fake a signal event. The number of background events was estimated by Monte Carlo simulation. We generated $K_L^0 \to \pi^0\pi^0$decays with 10 times larger statistics than the data. After imposing all the cuts, the background level was estimated to be 0.14. Table 2 summarizes the estimation for each background sources. Distribution in the P_T vs reconstructed Z position plane is shown in Figure 4. In this plots, number of events outside the signal box is well estimated by our Monte Carlo simulation.

6. Sensitivity and results

After determining all the selection criteria and estimating background levels, we examined the events in the signal box and found no candidates, as shown in Figure 5.

The number of collected K_L^0decays was estimated using the $K_L^0 \to \pi^0\pi^0$ decay, based on 1072 events, and was cross-checked by measuring $K_L^0 \to \pi^0\pi^0\pi^0$ and $K_L^0 \to \gamma\gamma$ decays [7]. Thus, we

PoS(KAON09)046

Background source	Estimated number of background
CC02	0.15 ± 0.05
CV	$0.0\ (< 0.15)$
CV-η	0.14 ± 0.07
$K_L^0 \to \pi^0\pi^0$	0.14 ± 0.05
$K_L^0 \to \pi^- e^+ \nu$	$(4.7 \pm 0.7) \times 10^{-3}$
total	0.44 ± 0.10

Table 2: Estimated numbers of background events inside the signal box.

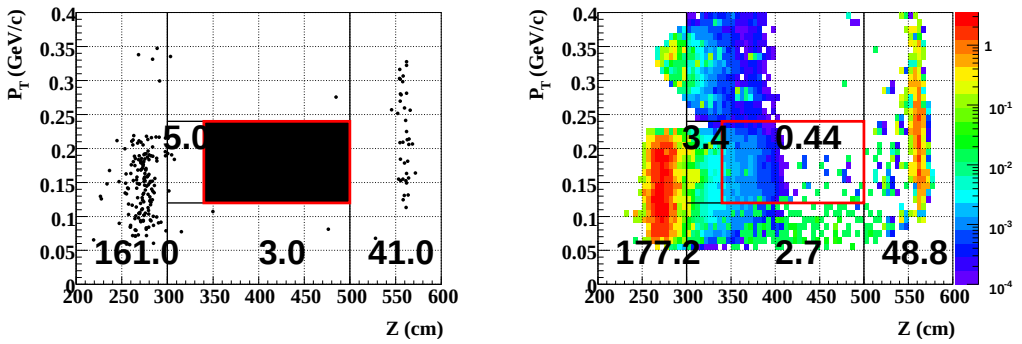

Figure 4: Scatter plot of P_T vs reconstructed Z position after imposing all cuts. Left plot shows for the Run-3 data, with signal region masked. Right plot shows the estimated background by simulation including halo neutron-induced and $K_L^0 \to \pi^0\pi^0$ backgrounds. Numbers in plots shows the number of events in each region. Normalization is done by ratio between data and MC in upstream region, with varying cuts and taking average of them.

obtained 3.48×10^9 K_L^0 decays in the decay volume. The single event sensitivity for the $K_L^0 \to \pi^0\nu\bar{\nu}$ branching ratio is given by

$$S.E.S.(K_L^0 \to \pi^0\nu\bar{\nu}) = \frac{1}{Acceptance \cdot N(K_L^0 decays)},$$

where the acceptance includes the geometrical acceptance, the analysis efficiency, and the acceptance loss due to accidental hits. Using the total acceptance of 0.98% and the number of K_L^0decays of 3.48×10^9, single event sensitivity was 3.0×10^{-8}.

Since we observed no events inside the signal box, we set an upper limit for the $K_L^0 \to \pi^0\nu\bar{\nu}$ branching ratio,

$$Br(K_L^0 \to \pi^0\nu\bar{\nu}) < 6.8 \times 10^{-8} (90\% C.L.),$$

based on Poisson statistics.

In near future, we are planning to combine Run2 data to Run3 data. Since we didn't see inside the box both for Run2 and Run3 during optimization for the event selection, we can apply new event selection to Run2 case.

PoS(KAON09)046

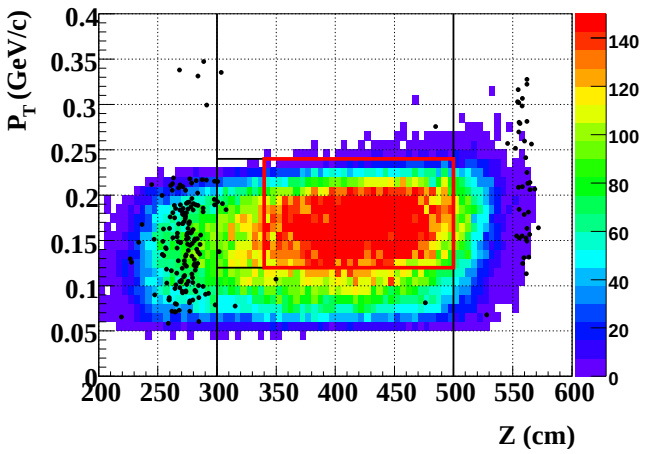

Figure 5: Scatter plot of P_T vs reconstructed Z position after imposing all the cuts. The points show the data and the colored contour represents the simulated distribution of the signal. The rectangle indicates the signal region.

References

[1] L. S. Littenberg, Phys. Rev. D **39**, 3322 (1989).

[2] F. Mescia and C. Smidth, Phys. Rev. D **76**, 034017 (2007).

[3] A. Alavi-Harati *et al.*, Phys. Rev. D **61**, 072006 (2000).

[4] J. K. Ahn *et al.*, Phys. Rev. Lett. **100**, 201802 (2008).

[5] H. Watanabe *et al.*, Nucl. Instr. Meth. Phys. Res., Sect. A **545**, 542 (2005).

[6] J. K. Ahn *et al.*, Phys. Rev. D **74**, 051105(R) (2006).

[7] The branching ratio of each K_L^0 decay mode was taken from W.-M. Yao *et al.*, (Particle Data Group), J. Phys. G **33**, 1 (2006) ; http://pdg/lbl.gov/ .

PoS(KAON09)046